Quantifying sheet wash erosion rates in a mountainous semi-arid basin using environmental radionuclides and a stream power model

Haopeng Geng [a], Baotian Pan [a*], David G Milledge [b], Bo Huang [a], Guoliang Zhang [a]

[a] *Key Laboratory of Western China's Environmental Systems, Ministry of Education, Lanzhou University, Lanzhou, PR China*

[b] *Department of Geography, Durham University, Durham, UK*

[*] Corresponding Author: Baotian Pan

Email address: panbt@lzu.edu.cn

Postal address:

Room 304,Key Laboratory of Western China's Environmental Systems (MOE)

Lanzhou University

No222 South of Tianshui Road

Lanzhou, Gansu 730000

PR China

Tel.: +86 931 8912315

Fax: +86 931 8912330

This article has been accepted for publication and undergone full peer review but has not been through the copyediting, typesetting, pagination and proofreading process, which may lead to differences between this version and the Version of Record. Please cite this article as doi: 10.1002/esp.3761

ABSTRACT: Erosion rates and processes define how mountainous landscapes evolve. This study determines the range of erosion rates in a semi-arid landscape over decadal time spans and defines the dominant processes controlling variability in erosion rates. The varying topography and climatic regimes of the Xiying Basin (Qilian Shan Mountains, China) enables us to examine the relative roles of sheet wash versus rainsplash and the influence vegetation on soil erosion and deposition. Soil erosion rates since 1954 were determined using ^{137}Cs along 21 transects at 4 sites with varying gradient, rainfall, and vegetation cover. The mean ^{137}Cs derived soil erosion rate ~0.42 mm/a, consistent with the catchment level erosion rate derived from total sediment yield for a 44 year record. However, there is considerable variability in ^{137}Cs erosion rates both between transects and along transects. Perhaps reflecting variation not only in the effectiveness of individual processes but also in their relative roles. We compare the ^{137}Cs-derived erosion rates with 1-D models for sediment flux that incorporate sheet wash and rainsplash processes, testing them over a previously untested 60 year timescale. The variability in ^{137}Cs erosion rates along transects is best replicated by sheet wash dominated simulations, suggesting that this is the dominant erosion process in this semi-arid landscape. The functional form of the sheetwash model can also explain our observations that ^{137}Cs erosion rates decrease with upslope length (i.e. distance down slope) while its

variability increases. However, sparsely vegetated sites, located in slightly drier locations, have higher erosion rates, and are not as accurately modeled as densely vegetated sites, suggesting that patchiness of vegetation introduces fine scale variability in erosion rates on these slopes.

KEYWORDS: erosion rate; ^{137}Cs; sheet wash; rainsplash; Qilian Shan Mountains

Introduction

Many studies report basin scale erosion rates over timescales from years (Gabet et al., 2008; Pan et al., 2010) to millennia (DiBiase et al., 2010; Ouimet et al., 2009) and explain these erosion rates in terms of broad topographic, tectonic or climatic characteristics (Aalto et al., 2006). However, mountainous catchments generally comprise many processes including fluvial processes, soil creep, rainsplash and overland flow (Dietrich and Dunne, 1978), as well as some episodic processes (Hales and Roering, 2005; Larsen and Montgomery, 2012; Stock and Dietrich, 2006). The quantitative study of process rates is difficult since these rates are highly variable over short spatial and temporal-scales making short-term and/or basin averaged estimates problematic. An alternative approach is to investigate the spatial variability of erosion rates within a catchment and use these to infer the processes that are responsible for them.

Our focus is the mountainous and semi-arid Xiying Basin in the eastern Qilian Shan Mountains where mean local relief (mean slope) is known to be an important control on decadal-scale basin-wide erosion rates (Pan et al., 2010). While the Xiying basin is subject to a suite of erosion processes we focus on soil mantled slopes with angles less than 40˚ (i.e. transport limited slopes not dominated by mass movement) since these make up ~90% of the basin by area (Geng, 2014). Abrahams et al. (1994) suggest that overland flow is one of the dominant processes governing the evolution of semi-arid landscapes, and observations in the Xiying Basin during storm events suggest that overland flow is common in many areas of the basin. The runoff-dominated annual variation in sediment flux from this and other neighboring basins (Pan et al., 2010) indicate that rainstorm related processes (rainsplash and overland flow) may be the dominant erosion processes. However, we do not know how much erosion can be attributed to these processes, or how this varies spatially within the basin. In this paper we aim to address these questions.

In semi-arid landscapes like the Xiying basin, overland flow is generated when the rainfall intensity exceeds the infiltration capacity of the soil (Horton, 1945). As water flows over the soil surface it exerts a shear stress on soil particles, and if this stress exceeds the critical shear stress of the particles they are mobilized and transported downslope. Vegetation provides additional

strength to the soil increasing the critical shear stress (Prosser et al., 1995). Shear stress is influenced by surface roughness, local gradient, and water discharge which in turn is a function of upslope contributing area, rainfall intensity and infiltration rate (Dunne and Dietrich, 1980; Prosser and Rustomji, 2000). Under a set of simplifying assumptions (Howard, 1994), these relationships reduce to the stream power equation, which provides a simple way to express the sediment flux due to overland flow. The impact of the raindrops themselves also mobilise sediment and the particles travel further in a downslope than upslope direction resulting in a net downslope flux of material proportional to the local slope (Dunne, 1980). This rainsplash process can be shown both from theory (e.g. Furbish et al., 2009) and observation (e.g. Dunne et al., 2010) to be well approximated by linear diffusion. Both rainsplash and sheet wash act on the slope to transport sediment during a rainstorm but their contribution differs with location on the slope (Dunne and Aubry, 1986). Previous research has attempted to identify topographic fingerprints of these processes by comparing predictions from process models with observed topographic form, often assuming topographic steady state (Gilbert, 1909; Kirkby, 1971; Perron et al., 2009; Roering et al., 2007). Booth and Roering (2011) also successfully incorporated earth flow flux with diffusive processes (soil creep) and overland flow to investigate the dominant transport processes in soil-mantled hillslopes. We take a similar

approach, using a model that can represent both rainsplash and sheet wash processes, we advance on previous work by comparing erosion predictions with observed soil erosion rates rather than topographic profiles since this approach allows us to relax the assumption of topographic steady state.

To quantify the water-induced sediment flux requires long-term observations to integrate the effects of episodic storm events (Baffaut et al., 1996). Experimental plots can provide reliable hillslope sediment flux estimates at annual or even decadal scales (Gifford, 1973), but it is difficult to record sediment detachment and transport rates along hillslopes. Magnetic material (Parsons et al., 1993) and rare earth elements (Matisoff et al., 2001) have been successfully used as indicators to trace sediment transport along a hillslope during individual rainfall events. However, here our aim is to examine soil redistribution rates over decadal timescales.

Fallout ^{137}Cs provides a tracer that is particularly well suited to applications over these timescales and as a result has been widely used for studying decadal-scale soil erosion and sediment delivery without requiring long-term observation (Ritchie and McHenry, 1990; Walling et al., 1996). ^{137}Cs is an anthropogenic radionuclide generated as a product of nuclear weapons testing, primarily from the mid 1950s to the late 1960s (Walling and He, 1992). In predominantly mineral soils ^{137}Cs fallout is rapidly and strongly adsorbed by the soil particles at or near the ground surface (Tamura, 1964). Where this is

the case, subsequent redistribution of ^{137}Cs is associated with movement of those soil particles, and since the ^{137}Cs fallout is predominantly at the ground surface it is particularly susceptible to water-induced soil erosion (Ritchie et al., 1974). This strong connection to water-induced erosion and the timescale since initial fallout, which is long enough to integrate over the effects of individual storms, makes ^{137}Cs particularly suitable as a tracer for soil erosion by surface runoff (Loughran et al., 1990).

The ^{137}Cs technique has also been used to validate the results of erosion models or calibrate model parameters (Alatorre et al., 2012), such as RUSLE (López-Vicente et al., 2008) and WATEM/SEDEM (Feng et al., 2010). However, while the ^{137}Cs technique has been widely applied in agriculture landscapes across a broad climatic regime (Govers et al., 1996; Nagle et al., 2000; Poręba and Bluszcz, 2007; Soto and Navas, 2008; Sutherland, 1992) it has rarely been applied to natural landscapes (with exceptions like Albers and Rackwitz, 1998; Kaste et al., 2006).These natural landscapes, which are our focus, have been represented in simple process based models that have been tested over long (>1ka; McKean et al., 1993) and short timescales (<1yr; Nearing et al., 1997). Fallout nuclides enable us to test them at an intermediate (~50 yr) timescale at which they have not previously been tested. Examining the model structure and parameters required to explain the ^{137}Cs-derived soil erosion rates then enables us to identify the dominant

rainstorm related processes in our landscape and how they are influenced by topography and climate.

To achieve this aim our objectives are: 1) to estimate decadal scale erosion rates for semi-arid soil mantled hillslopes under a range of topographic conditions and across a climatic gradient; 2) to examine the relationship between erosion rates, topographic conditions and climate driven site properties (vegetation cover and rainfall); and 3) to compare the ability of rainsplash and overland flow to explain ^{137}Cs-derived erosion patterns both within and between individual transects. To do this we will use the ^{137}Cs technique to examine soil erosion rates in the Xiying Basin. Four study sites were chosen on soil-mantled slopes with varying gradients and spanning an elevation range of about 2000 m and several vegetation zones. We then use a simple 1-D model to predict soil erosion rates across the study transects to examine the influence of climatic regimes and topography on overland flow erosion.

Geologic and geographic setting

The Qilian Shan Mountains, located along the northeast margin of the Tibetan Plateau, have been experiencing intense tectonic deformation since the late Cenozoic (Tapponnier et al., 2001). Active uplift ~12 Ma B.P. resulted in a shift to more arid conditions (Dettman et al., 2003), which may have been

enhanced during the Quaternary (Wu et al., 2007). Contrary to the global trend these arid conditions have remained despite Holocene warming and deglaciation (Chen et al., 2001). Summer monsoon and westerlies both affect this area, leading to a semiarid climatic regime (Wang et al., 2010). The Xiying Basin is a small drainage basin in the eastern Qilian Shan Mountains (Figure 1). Observations in the Xiying Basin show that mean annual temperature decreases linearly and rainfall (Figure 1) generally increases linearly with elevation (Pan et al., 2010).

There is strong vertical zonation to the vegetation in the basin due to its high relief (>3000 m) and steep climatic gradient. Arid/semi-arid grasslands occupy the area below about 2600 m and the tree line is about 3400 m. Alpine rhododendron shrubs and sub-alpine meadow vegetation grows above the tree line. The ground becomes largely barren above 3800 m, although alpine cushion vegetation can still inhabit above 4000 m. However, steppe and grassland are the dominant ecosystems, and supervised classification of *NDVI* (normalized difference vegetation index) using support vector machines indicates that alpine/sub-alpine steppe and arid/semi-arid grassland occupy around 60% of the study basin. More specifically in Figure 1, the study site AS (Alpine Steppe) is located at the transition elevation between the barren ground and alpine steppe, which are typically found at 3000 m – 3800 m. The MS (Mountain Steppe) is located above the arid/semi-arid grasslands and

below the tree line. The other two sites, MG (Mountain Desert Grassland) and DG (Desert Grassland), are arid/semi-arid grasslands found above 2000 m. All of our study sites have been subject to low density grazing by sheep and cattle for at least the last 100 years.

Methods and materials

The sampling strategy is established to capture the erosion distribution throughout the study area using the ^{137}Cs technique. There has been extensive recent discussion of the assumptions associated with using ^{137}Cs to measure soil redistribution rates (Mabit et al., 2013; Parsons and Foster, 2011). The key assumptions associated with this approach are that: 1) atmospheric fallout is spatially uniform; 2) the subsequent transfer of this fallout to the soil is also spatially uniform; and 3) the fallout is rapidly and near-irreversibly adsorbed onto soil particles. Under these conditions it is reasonable to assume that the redistribution of fallout is due to movement of soil particles across the soil surface.

We inventory fallout nuclides from a local reference site with 20 soil cores and adjust our observations to account for the local rainfall gradient in order to minimise the risk that the first assumption is violated. The extent to which the second and third assumptions are met introduces uncertainty into the estimated erosion rates, but this uncertainty is difficult to quantify. Given that

even very small amounts of mineral matter are capable of strongly sorbing ^{137}Cs (Shand et al., 1994), we think these assumptions are reasonable for our study area. The distribution of ^{137}Cs fallout with depth through the soil profile is well captured by the diffusion and migration model described below. This model provides a rational explanation for the observed ^{137}Cs distribution rather than a precise mechanistic representation. Although measurement error is well constrained, errors associated with model assumptions are less well constrained. Previous studies suggest that the error introduced by the ^{137}Cs technique is on the order of 5% - 10% (Basher, 2000; Kaste et al., 2006; Porto et al., 2011).

Sampling

To examine the influence of climatic regimes or topographic characteristics on overland flow erosion, we selected one reference site and four erosion sites characterized by varied land cover. Each site contained five or six transects of different gradients and each transect extended from the ridge to a break in slope. An Eijkelkamp split tube sampler with a soft PVC sample liner (diameter 50 mm) was used to collect soil samples. Undisturbed bulk or sectioned samples can be drilled easily by an impact absorb hammer and be held in the sample liner.

Reference site

The reference inventory should represent the local fallout input under the assumption of spatially uniform fallout and no soil erosion (Owens and Walling, 1996). Such locations are rare in a landscape of dissected terrain, where even the interfluves are sharp ridge crests. However, there is an undissected surface located at the interfluve between the Xiying Basin, and the western neighboring basin (Pan et al., 2007). MGZ (Figure 1 and S1) is an undisturbed spot at the undissected surface with minimal slope and no evidence of erosion or deposition, making it an ideal reference site in the study area. At this site we collected 20-sectioned cores to the depth of ca. 400 mm within a 15m × 15m square area (inset photo in Figure S1). All the cores were sectioned at 10 mm intervals, and the sub-samples at the same depth in each core were amalgamated into a single composite sample to capture the vertical distribution of ^{137}Cs.

Erosion sites

We chose 4 sites (Figure 1, Table 1) to sample a range of land cover types across the vertically zoned vegetation distribution in the Xiying Basin: AS (Alpine Steppe), MS (Mountain Steppe), MG (Mountain Desert Grassland), DG (Desert Grassland). At each site we chose 5 or 6 transects with similar aspects that had a continuous soil mantle, but had different gradients to

capture the topographic influence (Table 1, Figure 2). Plan curvature close to zero ensures that each sampling point along the transect receives flow from only those points immediately upslope, while profile curvature close to zero (mean curvature varied from -0.0038 – 0.002 m^{-1}) ensures a constant slope gradient along the profile (Figure S2 - 5). We calculated *Normalised Difference Vegetation Index* (*NDVI;* Kriegler et al., 1969) to distinguish the difference in vegetation cover between these transects and rescale the range from 0 to 1 (Table 1). *NDVI* was calculated using Landsat TM5 (09/08/2010) based on the equation: *NDVI = (Band 4 - Band 3) / (Band 4 + Band 3)* (Rouse et al., 1974).

On each transect, bulk samples of the top 200 mm of soil were collected at 5 m intervals along a single line from the ridge in a downslope direction. The topographic gradients of each transect were surveyed on-site at the same interval (5 m). At three of these sites (AS, MG, DG), the slope length is 50 m (measured parallel to the soil surface) after which curvature begins to change. At the MS site, however, we varied the slope length (60 m - 110 m) to investigate its influence on erosion rate. We convert all slope lengths into planimetric coordinates for our analysis (transect length, Table 1). All the samples were collected during the later rain season from middle September to early October in 2010.

Laboratory analysis

The bulk and sectioned samples were pre-treated using the standard procedures to air-dry, disaggregate (crush the soil) and sieve through a 2 mm mesh (Walling et al., 2003). The measurements of ^{137}Cs concentration were undertaken on 200g soil samples of grain size < 2 mm at the School of Nuclear Science and Technology at Lanzhou University, using a high-resolution, low background N-type HPGe coaxial detector (ORTEC, GMX-30P). For the gamma spectrometry measurements, each sample was counted ca. 12 h to detect the gamma ray peak at 662 keV for ^{137}Cs. The net count rates were calculated as the ratio of the total net counts covering 15 channels around the channel located at 662 keV to the count time, providing an averaged analytical precision of ±4% at the 95% significance level. The ^{137}Cs concentration (mBq/cm^3) of each sample was calculated using the net count rate, mass and density for the sample and the detector efficiency and net count rate of the standard ^{137}Cs sample. The ^{137}Cs inventories (Bq/m^2) were the product of ^{137}Cs concentration and sampling depth.

Conversion model

Quantitative estimates of soil erosion using ^{137}Cs require a model to convert the bulk ^{137}Cs inventory in the soil to an erosion or deposition rate (Walling and He, 1999). Simple empirical (often exponential) functions can be obtained

from observed relationships between soil erosion and ^{137}Cs loss from experimental plots (Ritchie et al., 1974; Rogowski and Tamura, 1965). They are easy to apply but rely on experimental research, which is hard to extrapolate to natural slopes (Walling and He, 1999).

For undisturbed natural slopes with long-term water-induced soil erosion, the diffusion and migration model is a more realistic approach, which can account for the time-dependent ^{137}Cs fallout (Walling et al., 2003; Walling and He, 1999). A partial differential equation is used to describe the effective advective-diffusive process and represent ^{137}Cs variation with both time and soil depth.

$$\frac{\partial C_u(z,t)}{\partial t} = D \cdot \frac{\partial^2 C_u(z,t)}{\partial z^2} - V \cdot \frac{\partial C_u(z,t)}{\partial z} - \lambda \cdot C_u(z,t) \quad (1)$$

Where $C_u(z,t)$ is the ^{137}Cs concentration (mBq/cm^3), z is the depth (mm), t is the time (year), λ is the ^{137}Cs decay constant (0.023/a), D (mm^2/a) is the diffusion coefficient and V (mm/a) is the downward advection rate. The model application requires the decomposition for the linear one dimensional time dependent partial differential equation. To do this we solved the diffusion and migration model partial differential equation numerically, using a forward finite difference scheme with a spatial resolution of 1 mm over a 500 mm domain and a no flux condition on the upper and lower boundaries (He and Walling, 1997). The ^{137}Cs input from fallout was assumed to begin in 1954, end in 1983 and follow the temporal distribution of monitoring station records from

the northern hemisphere (Cambray et al., 1989). The annual ^{137}Cs flux I(t) (Bq/m^2) was assumed to have the same relative annual variation of the monitoring stations records and was generated from the measured inventory at the reference site using the decay equation of ^{137}Cs (Walling et al., 2011). This initial input of annual flux was distributed within the relaxation depth H, the top 5 mm of the soil profile (He and Walling, 1997).

Results

The diffusion and migration model was employed to calculate the erosion rates at the study transects. The water-induced soil erosion or deposition rate at a point is calculated by comparing its depth integrated ^{137}Cs inventory with that of a reference point (Walling and Quine, 1990): excess inventory indicates deposition of ^{137}Cs rich surface soil, while a reduction indicates its removal by erosion.

Vertical ^{137}Cs profile at the reference site

At the reference site (MGZ, Figure 1), ^{137}Cs fallout is found in the upper 180 mm of the soil profile with a total inventory of 5230 Bq/m^2, and its concentration shows a quasi-exponential decline with depth below the maximum value at 30 mm depth (Figure 3). The peaks (top 20 - 55 mm) are broad, with a half-height width of ca. 70 mm. The ^{137}Cs profile is typical of

those at undisturbed sites (He and Walling, 1997). The high spatial resolution of the observed ^{137}Cs profile (10 mm) allowed us to determine the advection of ^{137}Cs from the surface into the soil profile at a rate V = 0.79 ± 0.05 mm/a, and diffusion over time at a rate D = 20.8 ± 2.1 mm^2/a, both with a significance level of 95%. Although the model does not perfectly match the maximum ^{137}Cs value at 30 mm depth, it doesn't under or overestimate the inventories, provides a good representation of the penetration depth and captures the general form of the observed profile (Figure 3).

Total fallout is expected to increase slightly with mean annual rainfall due to wet deposition (Davis, 1963). The mean annual rainfall in Xiying Basin ranges from 235 mm/a to 565 mm/a across the sample sites (Figure 1, Table 1), which results in an estimated 28% decrease in reference inventory from AS to DG based on the model of Walling et al. (2011). Since it was not possible to find suitable reference sites for all four erosion sites due to the dissected topography, we extrapolated these inventories from the MGZ inventory (Table 1) using Walling et al.'s model (Walling et al., 2011). This model predicts fallout on the basis of latitude, longitude and average annual rainfall from 92 global observations, with an R^2 of 0.83 (Walling and He, 2000). We calculate the site specific reference inventories using Walling's model scaled to the MGZ reference inventory.

Soil erosion conversion

In order to compare bulk inventories along the transects with the reference inventory we must assume uniform values of the diffusion coefficient *D* and advection rate *V* across the basin. While we expect some variability in these coefficients between sites, we expect limited variability within a site and thus the associated error should be small relative to other uncertainties discussed below. Where ^{137}Cs is removed by erosion from the soil surface, the inventory loss at that point can be calculated by integrating the product of erosion rate *R* (mm/a) and surface ^{137}Cs concentration over time *t* according to Eq. 2 (Walling and He, 1999):

$$\int_o^t PRC_u(t')e^{-\lambda(t-t')}dt' = A_{u,ls}(t) \quad (2)$$

where $C_u(t')$ (mBq/cm^3) is the ^{137}Cs concentration in the surface soil at time *t'*, *P* is the particle size correction factor which is defined as the ratio of the ^{137}Cs concentration of mobilized sediment to that of the original soil, and $A_{u,ls}(t)$ (Bq/m^2) is the difference between the ^{137}Cs inventory at the reference site A_{ref} (Bq/m^2) and the inventory A_u (Bq/m^2) at that point.

Eq. 2 can be used to estimate the soil erosion rates at a point by comparing its bulk ^{137}Cs inventory with the reference inventory. Removal of surface soil will alter the upper boundary condition; erosion will result in upward movement of the profile especially for the peak ^{137}Cs concentration. This effect may be negligible where erosion rates are low but important where they

are high. We addressed this by defining a relationship between ^{137}Cs inventory and erosion rate that accounts for the removal of surface soil. We simulated the remaining ^{137}Cs inventory of soil within the diffusion and migration model by removing soil from the upper boundary. We employ this erosion-dependent surface soil concentration model to simulate the vertical profiles under a range of erosion rates. After 56 years of simulation (1954-2010), we integrated the concentrations by depth and obtained a series of remaining ^{137}Cs inventories with their corresponding erosion rates. This defines an exponential relationship between the remaining ^{137}Cs inventory and soil erosion rate (Figure 4). The exponential relationship is similar to the relationship generated by empirical models (Walling and Quine, 1990), but differs from the linear relationship predicted when the upper boundary condition does not account for soil erosion (Kaste et al., 2006; Walling and He, 1999).

Deposition rates can be determined from the ^{137}Cs inventory if the inventory of upslope locations is also known though there is no simple universal relationship between inventory and deposition rate. Since any excess ^{137}Cs in the inventory at an observation point $A_{u,ex(t)}$ ($A_u - A_{ref}$, Bq/m^2), is a function of the soil deposition rate (R', mm/a) and the concentration of ^{137}Cs in the soil being deposited ($C_{d(t')}$, mBq/cm^3) (Walling and He, 1999) we must calculate their deposition rates using:

$$\int_o^t R' C_d(t') e^{-\lambda(t-t')} dt' = A_{u,ex}(t) \quad (3)$$

We use erosion-dependent ^{137}Cs concentrations in the surface soil upslope of the observation point to calculate the ^{137}Cs concentration in the deposited sediment (*Cd(t')*, mBq/cm^3). The concentration of ^{137}Cs in the soil being deposited at the observation point is the erosion-weighted mean of the ^{137}Cs concentration of surface soil in the upslope contributing area for the current observation point. As a result while ^{137}Cs inventory will generally increase with deposition rate, this relationship is not universal but instead dependent on the concentration of the deposited soil and therefore the pattern of erosion upslope.

^{137}Cs erosion and controlling factors

The mean inventories for the 21 transects in Xiying Basin, including their ranges, are listed in Table 1. The varied reference inventories at four study sites (Table 1) were used to calculate the ^{137}Cs loss at each sampling point. Mean soil erosion rates (Table 1, Figure S6 - S10) for the 21 transects were calculated adopting the parameters at the reference site (MGZ). The majority of transects experienced some deposition (with one exception: AS32, Figure S6). In addition, we calculated another two sets of rates (Table 1) using the parameters for the upper/lower confidence bounds for the reference site. The results show a mean soil erosion rate of 0.42 mm/a for the 21 transects

throughout Xiying Basin. For the four sites, AS, MS, MG, DG, the mean soil erosion rates are 0.40 mm/a, 0.34 mm/a, 0.51 mm/a and 0.44 mm/a, respectively.

The spatial variation in ^{137}Cs erosion rates allows us to examine the controls on this variation between transects and within transects. Gradient and upslope length are two important topographic attributes that influence overland flow erosion (Horton, 1945; Howard, 1994). Figure 5A shows that for individual sample points there is considerable variability in erosion/deposition rates, even between points with the same gradient. This might be expected given both measurement uncertainty and the influence of local factors such as vegetation cover or micro-topography. However, once binned by gradient (0.1 m/m bins) the average erosion rates show a strong positive correlation with gradient (Figure 5A), which is supported by a similar relationship for transect averaged erosion rates and gradient (Figure 5B).

There is also considerable scatter in the relationship between upslope length and erosion rate. However, the mean erosion rates binned by upslope length (5 m bins) are negatively correlated with upslope length over the first 35 m, where data is available from all sites (Figure 5C). Larger upslope lengths are more difficult to interpret since the number of samples decreases with upslope length, introducing potential bias. This reduction in erosion rate with upslope length is unintuitive and is not the result of co-variance between gradient and

upslope length (Figure S11). However, it is possible under transport limited conditions if the divergence of the sediment flux decreases downslope, and we will discuss the conditions that might lead to this in the model simulation section. In terms of climatic factors, rainfall intensity and land cover (which is climate dependent) will strongly influence the overland flow generation and flow resistance (Prosser et al., 1995). Our results show a negative relationship between mean annual rainfall and erosion rates when comparing the four sites (Figure 5D), which is consistent with other observations in semi-arid areas (Langbein and Schumm, 1958). Our results also show a slight negative correlation between site-averaged erosion rates and *NDVI* (Figure 5E). The *NDVI* represents the amount of above ground biomass and could be influenced by annual rainfall. A larger *NDVI*, implies more vegetative cover, which will enhance the ground's capacity to resist erosion (Liu and Singh, 2004; Prosser et al., 1995).

Modeling the sheet wash and rainsplash erosion processes

The strong dependence of ^{137}Cs erosion on transect gradient could be explained by either wash erosion by water flowing over the surface or rainsplash. To establish which of these processes dominates, we developed

models for overland flow and rainsplash erosion, and compared their predictions with our observations.

Model setup

The stream power equation has usually been used to directly represent the rate of bedrock incision by fluvial processes assuming detachment limited conditions (Howard and Kerby, 1983; Whipple and Tucker, 1999). However, it can also be derived as a sediment transport law for alluvial rivers or overland flow on hillslopes assuming transport limited conditions (Dietrich et al., 2003). In the hillslope case, by assuming that rainfall and infiltration rate are uniform along each transect, sediment flux q_{sw} (m^2/a) due to overland flow should be a function of the upslope length from the hilltop x (m) and local gradient S (m/m), following the stream power equation (Kirkby, 1971):

$$q_{sw} = k \cdot x^m \cdot S^n \quad (4)$$

in which k, m and n are fitted parameters. Under the same assumptions, sediment flux q_{sr} (m^2/a) due to rainsplash should be a linear function of local gradient S (m/m):

$$q_{sr} = d \cdot S \quad (5)$$

where d is the rainsplash diffusion coefficient (m^2/a). If the assumption that the system is transport limited is valid over decadal time-scales (56 years for

^{137}Cs technique), the surface lowering rate *(∂z/∂t)* is given by the divergence of the sediment transport flux, q_s (Howard, 1994);

$$\partial z/\partial t = \partial q_s/\partial x \quad (6)$$

Note that this transport limited derivation differs from the detachment limited derivation because here the lowering rate is given by the divergence of the sediment flux rather than the flux itself.

We will test three versions of the model: 1) sheet wash only ($q_s = q_{sw}$); 2) rainsplash only ($q_s = q_{sr}$); and 3) the combined flux ($q_s = q_{sw} + q_{sr}$). In the model, no flow and sediment flux is assumed at the upper boundary (the hilltop) and no profile curvature change is assumed at the lower boundary:

$$\partial z/\partial t|_{x=0} = 0 \quad (7)$$

$$\partial^2 z/\partial x^2|_{x=L_h} = \partial^2 z/\partial x^2|_{x=L_h-dx} \quad (8)$$

in which L_h (m) is the transect length and *dx* (m) is the simulation interval, which is the horizontal distance between neighboring points.

Model simulation at individual transects

We run the model to predict water-induced erosion for the 56 years between initial ^{137}Cs fallout and our sample collection. The initial topography 56 years ago is back calculated from the current topography using the ^{137}Cs erosion rates. The same simulations were performed using the current topography as an initial condition but the difference between these sets of simulations was

negligible. We calibrate the parameters (*k*, *m*, *n* and *d*) with a nonlinear least-squares procedure (Coleman and Li, 1996) using MATLAB's *lsqnonlin* function, which minimizes the residuals between the estimated ^{137}Cs erosion rates and those simulated over 56 years for each transect. We used Monte Carlo simulation to account for the uncertainty in the ^{137}Cs-derived erosion rates and the transect topography. We ran the model 500 times for each transect randomly sampling slope values with +/- 0.5˚ from the observed slope. During each simulation, we randomly sampled the ^{137}Cs inventory for each point on the transect from a uniform distribution with a $\pm$10% error to calculate the erosion rates. We expect that this is a worst case scenario for the error associated with ^{137}Cs technique and slope measurement error. The mean simulated overland flow erosion rates match the mean ^{137}Cs erosion rates fairly well for individual transects with their optimal parameters (Figure 6A). However, the two topographic exponents (*m* and *n*), vary widely between transects. To reduce the free parameters and examine the parameter behavior across the basin we assigned *m* and *n* their average values from Monte Carlo simulation of all transects (0.8 and 1.1, respectively). The standard error of the mean parameter values accounting for ^{137}Cs technique and slope measurement uncertainty is 0.005 and 0.009 for *m* and *n* respectively, suggesting that these mean values are fairly robust to this measurement uncertainty. The two mean values are close to those that have

been associated with sheet wash processes (m = 1, n = 1) described by Kirkby (1971) and consistent with our field observation that the sampled transects are subjected to surface wash without gullying.

This stream power model with the upslope length exponent m less than 1 can explain both the observed decrease in ^{137}Cs erosion rate and the increase in its variability with increasing upslope length. The surface lowering rate $(\partial z/\partial t)$ is equal to the divergence of the sediment transport flux (q_{sw} in Eq.6) and thus considering sheet wash alone the divergence of the stream power (Eq.4).

When $n \approx 1$ and m = 0.8, the Eq. 6 becomes (see the derivation of Eq. 9 in supplementary materials):

$$\frac{\partial z}{\partial t} = \frac{\partial q_s}{\partial x} = -0.8 \cdot k \cdot \frac{\partial z}{\partial x} \cdot x^{-0.2} - k \cdot x^{0.8} \cdot \left(\frac{\partial^2 z}{\partial x^2}\right) \quad (9)$$

For planar slopes the second term in Eq. 9 goes to zero and erosion rate increases with gradient and decreases with upslope length ($x^{-0.2}$). This is consistent with the observed decrease in ^{137}Cs erosion rate with increasing upslope length (Figure 5C). However, even a small amount of curvature, which fluctuates around zero, will introduce scatter into the predicted relationship between upslope length and erosion rate. The model predicts that this scatter in erosion rate should increase with upslope length ($x^{-0.8}$) consistent with the increasing variability in observed ^{137}Cs erosion rate with increasing upslope length for lengths < 40 m (Figure S12). While the scatter

continues to increase for longer upslope lengths this may be due to a reduction in the number of longer transects.

The simulated erosion rates still match the ^{137}Cs erosion rates well using mean values for the exponents *m* and *n*, and the optimal *k* values for individual transects (Figure 6B). The parameter *k* represents any non-topographic properties influencing the rate of sediment transport, such as rainfall intensity, soil erodibility, infiltration rate, surface roughness and vegetation cover (Prosser and Rustomji, 2000). Next we examine the influence of these non-topographic properties by constraining *k* to be spatially constant and using least-squares calibration to find a single optimal *k* for all transects. The mean simulated rates still capture the tendency of the mean ^{137}Cs rates using the constant parameters: $k = 0.002$, $m = 0.8$ and $n = 1.1$, for all transects (Figure 6C). However, the simulated rates span a narrower range and have more scatter. There is a considerable cost to assigning a uniform rather than transect varying *k* in terms of the model's ability to reproduce transect averaged erosion rates. This may reflect the importance of non-topographic local conditions in defining erosion rates for a particular transect and the risk of seeking parameter uniformity at all costs. However, while we have good reason to expect that *k* might vary between transects we can learn relatively little by simply allowing it to be calibrated as a free parameter. Instead we aim to find an explanation for its variability.

Rainfall and vegetation cover are highly variable over the study area and there is a good physical basis to expect them to influence erosion rates. The averaged erosion rates at the four sites show a negative correlation either with mean annual rainfall (Figure 5D) or *NDVI* (Figure 5E). Therefore, the climatic condition might explain a considerable amount of the remaining between site variation in soil erosion and therefore the coefficient *k*. The *NDVI* is more spatially distributed and easy to obtain for future application, rather than the rainfall distribution in a mountainous area. Given the higher *NDVI* site with denser vegetation cover and the higher mean erosion rates at sparsely vegetated than densely vegetated sites, we test the vegetation cover influence by replacing *k* with a new parameter k_b and introducing the site mean NDVI (NI_c) as a surrogate for vegetation cover (i.e. $k=k_b/NI_c$). We adopt constant parameters (k_b, *m, n*) for all the transects and apply the sediment flux function in the form:

$$q_s = (k_b/NI_c) \cdot x^m \cdot S^n \quad (10)$$

where NI_c is the site mean *NDVI* , which is 0.668, 0.585, 0.459, 0.457 for AS, MS, MG, DG, respectively.

Least-squares calibration of k_b, *m* and *n* as constants in Eq. 10 based on transect average ^{137}Cs erosion rates resulted in parameter values of: 0.001, 0.8 and 1.1 respectively. The mean simulated erosion accounting for land cover (Figure 6D) has a wider rate distribution than when *k*, *m* and *n* are held

constant (Figure 6C), but does not improve the correlation between predicted erosion rates and ^{137}Cs-derived rates. This is surprising given the negative correlation between site averaged erosion rate and *NDVI*. However, it suggests that the high mean rates at MG and DG may be due to their higher mean gradients (Figure 5F) rather than their lower vegetation cover. Accordingly, we attempted to explain whether it was influenced by another process. Rainsplash (Ellison, 1944) may be an important erosive process on these transects, particularly at short upslope lengths where overland flow will not be generated during every rainfall event (Onda et al., 2007). To test this, we run the model to predict rainsplash-induced erosion for the same 56 year period, with back calculated initial topography. We calibrate the diffusivity parameter (*d*) for each transect with the nonlinear least-squares procedure minimizing the residuals between simulated and ^{137}Cs-derived erosion rates for each transect.

Although rainsplash sediment flux depends linearly on gradient (Eq. 5), rainsplash erosion rate depends on the diversion of the flux (Eq. 6), and therefore on curvature. The simulated and ^{137}Cs-derived transect averaged erosion rates show very little agreement even with calibrated *d* (Figure 6E). ^{137}Cs-derived erosion rates are consistently higher than those predicted due to rainsplash and are not correlated with them, suggesting that rainsplash alone is a poor explanation for ^{137}Cs-derived erosion rates on our transects.

This is because erosion is only possible across the full transect if gradient increases downslope increasing transport capacity and allowing transport of both new sediment and that generated upslope. Without this convex curvature erosion will decrease and sediment may even be deposited downslope.

Finally, we include both rainsplash and sheet wash in our sediment transport equation and express the sediment transport rate q_s (m^2/a) as:

$$q_s = d \cdot S + k \cdot x^m \cdot S^n \quad (11)$$

We keep the topographic exponents (m = 0.8 and n = 1.1) and apply the model (Eq. 11) to find the constant d and k for all transects. However, the simulation results show that k is still about 0.002 and the diffusion coefficient d is about 0.006. Under these conditions, rainsplash flux exceeds sheet wash flux only for upslope lengths < 5m and is < 5% of the flux for upslope lengths exceeding 200 m. Accordingly transect averaged erosion rates are altered by < 5% by the inclusion of rainsplash in our model. This suggests that sheet wash rather than rainsplash is the dominant process on the study transects.

Model simulation at individual sampling points

Having examined the relationship between transect-averaged erosion, topography and land cover, we now consider the ability of the model to predict variability in erosion rates along individual transects. In this case, we also

predicted the ^{137}Cs inventory at each point. Figure 7 shows model results at MS36, which is the longest transect in our dataset.

Under the two different initial conditions, the simulated sheet wash erosion rates are the same (0.31 mm/a) and the simulated mean ^{137}Cs inventories are close to each other (Figure 7), which is reasonable given the short time span. There is large variability in the measured ^{137}Cs erosion and deposition rates over short length scales at MS36 (and many other transects see Figures S6 - 10). The sheet wash model does a reasonable job of reproducing the general pattern of erosion/deposition rates along MS36 and the mean erosion rate. However, the model is less able to explain the erosion rates at short upslope lengths and does not predict the extreme erosion and deposition rates. We have shown above that rainsplash should exert most influence on erosion rates at short upslope lengths. However, Figure 7A shows that it is no more able than the sheet wash model to predict the ^{137}Cs-derived erosion rates at short upslope lengths. The rainsplash model predicts a similar pattern of erosion with distance along transect to the sheet wash model, but with reduced variability and a consistent bias towards low erosion rates.

The variability in the measured ^{137}Cs erosion and deposition rates over short length scales cannot be captured by sheetwash or rainsplash models, which account only for topographic controls on erosion rate. We suggest that the misfit (Figure 8A) at extreme erosion or deposition rates might be due to the

patchy vegetation cover in these semi-arid environments. To investigate the land cover influence, we divide the 21 transects into two groups, dense vegetation sites (AS and MS) and sparse vegetation sites (MG and DG). The root-mean-square deviation (RMSD) at dense vegetation sites (Figure 8B) is considerably lower than that at sparse vegetation sites (Figure 8C).

Discussion

In this semi-arid mountainous basin, ^{137}Cs derived soil erosion rates range from 0.17 mm/a to 0.80 mm/a with a mean value of 0.42 mm/a. Much of the within and between transect variations can be explained by expected relationships with topography, while the mean erosion rate is similar to other measured erosion rates in the study area. In order to compare these erosion rates, we convert our soil erosion rates to bedrock erosion rates assuming a rock density of 2650 kg/m^3 and using the soil density of each individual sample (Table S1, mean = 870 kg/m^3). Under these assumptions, the equivalent mean bedrock erosion rates are about 0.12 mm/a, 0.11 mm/a, 0.16 mm/a, and 0.16 mm/a for AS, MS, MG and DG, respectively. The mean equivalent bedrock erosion rate of AS and MS (0.11 mm/a) is of similar magnitude to the catchment level erosion rate derived from total sediment yield for a 44 year record (0.09mm/a, Pan et al., 2010), both assuming the rock density is 2650 kg/m^3. The mean bedrock erosion rate also matches the

exhumation rate derived from the apatite fission-track (AFT) dating (0.11 mm/a) at MS since the Late Cenozoic (Pan et al., 2013).

In our study area many of the hillslopes are planar suggesting that sheet wash dominates over much of the slope. Our ^{137}Cs-derived erosion rates on these planar hillslopes indicate that rainsplash should indeed dominate only over the first 5 m of these slopes beyond which sheet wash becomes dominant (accounting for 95% of erosion). Previous studies found that diffusive processes are active from the ridge until the gully formation or landsliding (Booth and Roering, 2011; Dietrich et al., 1992; Fernandes and Dietrich, 1997; Roering et al., 2001). Accordingly, it seems surprising that the zone in which diffusive processes dominate is so short for our study transects without evidence of gullies or landslides. This may suggest that: the diffusive process is not linearly dependent on slope(Roering et al., 1999), though there is good theoretical basis for linear slope dependent rainsplash; or that rainsplash is not very efficient on vegetated slopes. An alternative interpretation might be that: 1) the system is not purely transport limited but depends on the production of mobilizable sediment (e.g. by rainsplash or biotic processes) over longer timescales; or 2) the slow but continuous diffusive processes are under represented relative to sheet wash over the short observation period provided by the ^{137}Cs technique.

Secondly, it is surprising that the study slopes have an overland flow signature for considerable lengths but no indication of gully development until further down slope. This may be the result of biotic processes that alter the surface either through sediment redistribution (e.g. by beetles) or vegetation re-growth (Moreno-de las Heras et al., 2011). These processes will act to counter the incision, smoothing perturbations in the surface (e.g. rills) or introducing perturbations (blockages) that promote deposition rather than erosion (Dunne and Aubry, 1986).

There is some evidence for such perturbations in the ^{137}Cs-derived erosion rates along individual transects. Although the model was able to predict net transect trends there remained considerable variability in erosion rates between points (Figure 7), especially for sparsely vegetated transects (Figures S6-10). As a result, the agreement between predicted and ^{137}Cs-derived erosion rates for densely vegetated transects is better than for the sparsely vegetated transects (Figure 8). These large mismatches at the sparsely vegetated transects, where the sheet wash model fluctuates between over and under predicting the ^{137}Cs erosion, could be attributed to patchiness in the vegetation cover. In semi-arid environments, bare ground may be easily erodible while that beneath vegetation patches is more resistant due to root reinforcement (Gyssels et al., 2005). Vegetation can also reduce the erosive energy of both rainspash and overland flow: reducing the

impact of raindrops (Hoffman et al., 2013), reducing the amount of overland flow due to increased infiltration and slowing its velocity due to the roughness imposed by vegetation (Saco and Heras, 2013).

Conclusion

We used the environmental radionuclide ^{137}Cs with a vertical diffusion and migration model to measure soil erosion rates along downslope transects at four sites across the Xiying Basin over 56-year period. The results suggest a mean soil erosion rate of 0.42 mm/a for the 21 transects and assuming a rock density of 2650 kg/m^3 this implies an equivalent bedrock erosion rate of about 0.14 mm/a. This rate is a similar magnitude to the catchment level erosion rate (sediment yield) and exhumation rate (AFT dating) in this area. In order to investigate the dominant sediment transport processes, we used a simple soil erosion model to simulate the sediment flux for each transect. Under spatially constant parameters (k = 0.002, m = 0.8 and n = 1.1), the mean simulated sheet wash erosion rates match the mean ^{137}Cs erosion rates well for 21 transects.

The sheet wash model consistently out-performed the rainsplash model, resulting in reduced misfit between predicted and ^{137}Cs-derived erosion rates. In the combined sheet wash and rainsplash model, rainsplash dominated only within 5 m of the ridge and altered transect averaged erosion rates by <

5%, suggesting that the study slopes are strongly influenced by sheet wash. The model performed better for densely vegetated transects than sparsely vegetated transects, where mismatches between predicted and ^{137}Cs-derived erosion rates might be attributed to the patchiness of vegetation. Our results suggest that overland flow is one of the dominant processes of erosion on the soil-mantled slopes of the Xiying Basin, that topography is a first order control on erosion rate but that variability in vegetation cover introduces fine scale variability in erosion rates along the slopes.

Acknowledgements—We thanks Xiaofei Hu, Bo Cao, Jun Wang, Yapeng Ji, Shaofei Jiang, Dongsheng Guan and Jundi Zhang for field work, and we also thanks Yu Zhang and Fenliang Liu for help with experiments. We are also grateful to William E. Dietrich for insightful suggestions. This research was financially supported by the Key Project of the Major Research Plan of the NSFC (91125008), the National Basic Research Program of China (2011CB403301), the National Natural Science Foundation of China (NSFC) for Distinguished Young Scholars (40925001), and the Fundamental Research Funds for the Central Universities (lzujbky-2015-128).

References

Aalto R, Dunne T, Guyot JL. 2006. Geomorphic controls on Andean denudation rates. *Journal of Geology* **114**: 85–99. DOI: 10.1086/498101

Abrahams AD, Parsons AJ, Wainwright J. 1994. Resistance to overland flow on semiarid grassland and shrubland hillslopes, Walnut Gulch, southern Arizona. *Journal of Hydrology* **156**: 431–446. DOI: 10.1016/0022-1694(94)90088-4

Alatorre LC, Beguería S, Lana-Renault N, Navas A, García-Ruiz JM. 2012. Soil erosion and sediment delivery in a mountain catchment under scenarios of land use change using a spatially distributed numerical model. *Hydrology and Earth System Sciences* **16**: 1321–1334. DOI: 10.5194/hess-16-1321-2012

Albers BP, Rackwitz R, Schimmack W, Bunzl K. 1998. Transect survey of radiocesium in soils and plants of two alpine pastures. *Science of The Total Environment* **216**: 159–172. DOI: 10.1016/S0048-9697(98)00150-8

Baffaut C, Nearing MA, Nicks AD. 1996. Impact of cligen parameters on WEPP-predicited average annual soil loss. *Transaction of the American Society of Agricultural and Biological Engineers* **39**: 447–457. DOI: 10.13031/2013.27522

Basher LR. 2000. Surface erosion assessment using 137Cs: examples from New Zealand. *Acta Geologica Hispanica* **35**: 219–228.

Booth AM, Roering JJ. 2011. A 1-D mechanistic model for the evolution of earthflow-prone hillslopes. *Journal of Geophysical Research* **116**: F04021. DOI: 10.1029/2011JF002024

Cambray RS, Playford K, Lewis GNJ, Campenter RC. 1989. Radioactive fallout in air and rain: results to the end of 1988. UK Atomic Energy Authority：Report no. AERE-R10155

Chen FH, Zhu Y, Li JJ, Shi Q, Jin LY, Wünemann B. 2001. Abrupt Holocene changes of the Asian monsoon at millennial- and centennial-scales: Evidence from lake sediment document in Minqin Basin, NW China. *Chinese Science Bulletin* **46**: 1942–1947. DOI: 10.1007/BF02901902

Coleman TF, Li YY. 1996. An Interior Trust Region Approach for Nonlinear Minimization Subject to Bounds. *Society for Industrial and Applied Mathematics Journal on Optimization* **6**: 418–445. DOI: 10.1137/0806023

Davis JJ. 1963. Cesium and its relationship to potassium in ecology. In *Radioecology*, Schultz V and Klement A (eds). Reinhold: New York; 539–556.

Dettman DL, Fang XM, Garzione CN, Li JJ. 2003. Uplift-driven climate change at 12 Ma: a long $\delta^{18}O$ record from the NE margin of the Tibetan

plateau. *Earth and Planetary Science Letters* **214**: 267–277. DOI: 10.1016/S0012-821X(03)00383-2

DiBiase RA, Whipple KX, Heimsath AM, Ouimet WB. 2010. Landscape form and millennial erosion rates in the San Gabriel Mountains, CA. *Earth and Planetary Science Letters* **289**: 134–144. DOI: 10.1016/j.epsl.2009.10.036

Dietrich WE, Bellugi DG, Sklar LS, Stock JD, Heimsath AM, Roering JJ. 2003. Geomorphic transport laws for predicting landscape form and dynamics. In *Prediction in Geomorphology*, Wilcock PR and Iverson RM (eds). American Geophysical Union: Washington, D. C.; 103–132. DOI: 10.1029/135GM09

Dietrich WE, Dunne T. 1978. Sediment budget for a small catchment in mountainous terrain. *Zeit. for Geomorph.N.F.* **Suppl. Bd.**: 191–206.

Dietrich WE, Wilson CJ, Montgomery DR, McKean J, Bauer R. 1992. Erosion thresholds and land surface morphology. *Geology* **20**: 675–679. DOI: 10.1130/0091-7613(1992)020<0675:etalsm>2.3.co;2

Dunne T. 1980. Formation and controls of channel networks. *Progress in Physical Geography* **4**: 211–239.

Dunne T, Aubry B. 1986. Evaluation of Horton's theory of sheet wash and rill erosion on the basis of field experiments. In *Hillslope Processe*, Abrahams AD (ed). Allen&Unwin: Boston; 31–53.

Dunne T, Dietrich WE. 1980. Experimental study of Horton overland flow on tropical hillslopes 1. *Zeit. for Geomorph.N.F.* **Suppl.Bd.**: 40–59.

Dunne T, Malmon D V., Mudd SM. 2010. A rain splash transport equation assimilating field and laboratory measurements. *Journal of Geophysical Research* **115**: F01001. DOI: 10.1029/2009JF001302

Ellison WD. 1944. Studies of raindrop erosion. *Agricultural Engineering* **25**: 131–136. DOI: 10.2307/302397

Feng XM, Wang YF, Chen LD, Fu BJ, Bai GS. 2010. Modeling soil erosion and its response to land-use change in hilly catchments of the Chinese Loess Plateau. *Geomorphology* **118**: 239–248. DOI: 10.1016/j.geomorph.2010.01.004

Fernandes NF, Dietrich WE. 1997. Hillslope evolution by diffusive processes: The timescale for equilibrium adjustments. *Water Resources Research* **33**: 1307–1318. DOI: 10.1029/97WR00534

Furbish DJ, Childs EM, Haff PK, Schmeeckle MW. 2009. Rain splash of soil grains as a stochastic advection-dispersion process, with implications for desert plant-soil interactions and land-surface evolution. *Journal of Geophysical Research* **114**: F00A03. DOI: 10.1029/2009JF001265

Gabet EJ, Burbank DW, Pratt-Sitaula B, Putkonen J, Bookhagen B. 2008. Modern erosion rates in the High Himalayas of Nepal. *Earth and Planetary Science Letters* **267**: 482–494. DOI: 10.1016/j.epsl.2007.11.059

Geng HP. 2014. Decadal-scale erosion based on sediment flux and environmental radionuclides in Qilian Shan Mountains, unpublished PhD Thesis (in chinese), Lanzhou University, Lanzhou, China; 163pp.

Gifford GF. 1973. Runoff and sediment yields from runoff plots on chained pinyon-juniper sites in Utah. *Journal of Range Management* **26**: 440–443.

Gilbert GK. 1909. The Convexity of Hilltops. *The Journal of Geology* **17**: 344–350.

Govers G, Quine TA, Desmet PJJ, Walling DE. 1996. The relative contribution of soil tillage and overland flow erosion to soil redistribution on agricultural land. *Earth Surface Processes and Landforms* **21**: 929–946. DOI: 10.1002/(SICI)1096-9837(199610)21:10<929::AID-ESP631>3.0.CO;2-C

Gyssels G, Poesen J, Bochet E, Li Y. 2005. Impact of plant roots on the resistance of soils to erosion by water: a review. *Progress in Physical Geography* **29**: 189–217. DOI: 10.1191/0309133305pp443ra

Hales TC, Roering JJ. 2005. Climate-controlled variations in scree production, Southern Alps, New Zealand. *Geology* **33**: 701–704. DOI: 10.1130/G21528.1

He Q, Walling DE. 1997. The distribution of fallout 137Cs and 210Pb in undisturbed and cultivated soils. *Applied Radiation and Isotopes* **48**: 677–690. DOI: 10.1016/S0969-8043(96)00302-8

Hoffman O, Yizhaq H, Boeken BR. 2013. Small-scale effects of annual and woody vegetation on sediment displacement under field conditions. *Catena* **109**: 157–163. DOI: 10.1016/j.catena.2013.04.003

Horton RE. 1945. Erosional development of streams and their drainage basins; hydrophysical approach to quantitative morphology. *Geological Society of America Bulletin* **56**: 275–370. DOI: 10.1130/0016-7606(1945)56[275:EDOSAT]2.0.CO;2

Howard AD. 1994. A detachment-limited model of drainage basin evolution. *Water Resources Research* **30**: 2261–2285. DOI: 10.1029/94WR00757

Howard AD, Kerby G. 1983. Channel changes in badlands. *Geological Society of America Bulletin* **94**: 739–752. DOI: 10.1130/0016-7606(1983)94<739:CCIB>2.0.CO;2

Kaste JM, Heimsath AM, Hohmann M. 2006. Quantifying sediment transport across an undisturbed prairie landscape using cesium-137 and high resolution topography. *Geomorphology* **76**: 430–440. DOI: 10.1016/j.geomorph.2005.12.007

Kirkby MJ. 1971. Hillslope process-response models based on the continuity equation. *Inst. Br. Geogr. Spec. Publ.* **3**: 15–30.

Kriegler FJ, Malila WA, Nalepka RF, Richardson W. 1969. Preprocessing transformations and their effects on multispectral recognition. 97–131 pp.

Langbein WB, Schumm SA. 1958. Yield of sediment in relation to mean annual precipitation. *Transactions, American Geophysical Union* **39**: 1076–1084. DOI: 10.1029/TR039i006p01076

Larsen IJ, Montgomery DR. 2012. Landslide erosion coupled to tectonics and river incision. *Nature Geoscience* **5**: 468–473. DOI: 10.1038/NGEO1479

Liu QQ, Singh VP. 2004. Effect of microtopography, slope length and gradient, and vegetative cover on overland flow through simulation. *Journal of Hydrologic Engineering* **9**: 375–382. DOI: 10.1061/(ASCE)084-0699(2004)9:5(375)

López-Vicente M, Navas A, Machín J. 2008. Identifying erosive periods by using RUSLE factors in mountain fields of the Central Spanish Pyrenees. *Hydrology and Earth System Sciences* **12**: 523–535. DOI: 10.5194/hess-12-523-2008

Loughran RJ, Campbell BL, Elliott GL, Shelly DJ. 1990. Determination of the rate of sheet erosion on grazing land using caesium-137. *Applied Geography* **10**: 125–133. DOI: 10.1016/0143-6228(90)90048-T

Mabit L, Meusburger K, Fulajtar E, Alewell C. 2013. The usefulness of 137Cs as a tracer for soil erosion assessment: A critical reply to Parsons and Foster (2011). *Earth-Science Reviews* **127**: 300–307. DOI: 10.1016/j.earscirev.2013.05.008

Matisoff G, Ketterer ME, Wilson CG, Layman R, Whiting PJ. 2001. Transport of rare earth element-tagged soil particles in response to thunderstorm runoff. *Environmental science & technology* **35**: 3356–3362. DOI: 10.1021/es001693m

McKean JA, Dietrich WE, Finkel RC, Southon JR, Caffee MW. 1993. Quantification of soil production and downslope creep rates from cosmogenic 10Be accumulations on a hillslope profile. *Geology* **21**: 343–346. DOI: 10.1130/0091-7613(1993)021<0343:QOSPAD>2.3.CO;2

Moreno-de las Heras M, Díaz-Sierra R, Nicolau JM, Zavala MA. 2011. Evaluating restoration of man-made slopes: a threshold approach balancing vegetation and rill erosion. *Earth Surface Processes and Landforms* **36**: 1367–1377. DOI: 10.1002/esp.2160

Nagle GN, Lassoie JP, Fahey TJ, McIntyre SC. 2000. The use of caesium-137 to estimate agricultural erosion on steep slopes in a tropical watershed. *Hydrological Processes* **14**: 957–969. DOI: 10.1002/(SICI)1099-1085(20000415)14:5<957::AID-HYP3>3.0.CO;2-6

Nearing MA, Norton LD, Bulgakov DA, Larionov GA, West LT, Dontsova KM. 1997. Hydraulics and erosion in eroding rills for stream power and sediment load fit the form of a logistic curve are total discharge. **33**: 865–876.

Onda Y, Kato H, Tanaka Y, Tsujimura M, Davaa G, Oyunbaatar D. 2007. Analysis of runoff generation and soil erosion processes by using environmental radionuclides in semiarid areas of Mongolia. *Journal of Hydrology* **333**: 124–132. DOI: 10.1016/j.jhydrol.2006.07.030

Ouimet WB, Whipple KX, Granger DE. 2009. Beyond threshold hillslopes: Channel adjustment to base-level fall in tectonically active mountain ranges. *Geology* **37**: 579–582. DOI: 10.1130/g30013a.1

Owens PN, Walling DE. 1996. Spatial variability of caesium-137 inventories at reference sites: an example from two contrasting sites in England and Zimbabwe. *Applied Radiation and Isotopes* **47**: 699–707. DOI: 10.1016/0969-8043(96)00015-2

Pan BT, Gao HS, Wu GJ, Li JJ, Li BY, Ye YG. 2007. Dating of erosion surface and terraces in the eastern Qilian Shan, northwest China. *Earth Surface Processes and Landforms* **32**: 143–154. DOI: 10.1002/esp.1390

Pan BT, Geng HP, Hu XF, Sun RH, Wang C. 2010. The topographic controls on the decadal-scale erosion rates in Qilian Shan Mountains, N.W. China. *Earth and Planetary Science Letters* **292**: 148–157. DOI: 10.1016/j.epsl.2010.01.030

Pan BT, Li QY, Hu XF, Geng HP, Liu ZB, Jiang SF, Yuan WM. 2013. Cretaceous and Cenozoic cooling history of the eastern Qilian Shan, north-eastern margin of the Tibetan Plateau: evidence from apatite fission-track analysis. *Terra Nova* **25**: 431–438. DOI: 10.1111/ter.12052

Parsons AJ, Foster IDL. 2011. What can we learn about soil erosion from the use of 137Cs? *Earth-Science Reviews* **108**: 101–113.

Parsons AJ, Wainwright J, Abrahams AD. 1993. Tracing sediment movement in interrill overland flow on a semi-arid grassland hillslope using magnetic susceptibility. *Earth Surface Processes and Landforms* **18**: 721–732. DOI: 10.1002/esp.3290180806

Perron JT, Kirchner JW, Dietrich WE. 2009. Formation of evenly spaced ridges and valleys. *Nature* **460**: 502–505. DOI: 10.1038/nature08174

Poręba GJ, Bluszcz A. 2007. Determination of the initial 137Cs fallout on the areas contaminated by Chernobyl fallout. *Geochronometria* **26**: 35–38. DOI: 10.2478/v10003-007-0009-y

Porto P, Walling DE, Callegari G. 2011. Using 137Cs measurements to establish catchment sediment budgets and explore scale effects. *Hydrological Processes* **25**: 886–900. DOI: 10.1002/hyp.7874

Prosser IP, Dietrich WE, Stevenson J. 1995. Flow resistance and sediment transport by concentrated overland flow in a grassland valley. *Geomorphology* **13**: 71–86. DOI: 10.1016/0169-555X(95)00020-6

Prosser IP, Rustomji P. 2000. Sediment transport capacity relations for overland flow. *Progress in Physical Geography* **24**: 179–193. DOI: 10.1177/030913330002400202

Ritchie JC, McHenry JR. 1990. Application of radioactive fallout cesium-137 for measuring soil erosion and sediment accumulation rates and patterns: a review. *Journal of environmental quality* **233**: 215–233. DOI: 10.2134/jeq1990.00472425001900020006x

Ritchie JC, Spraberry JA, McHenry JR. 1974. Estimating soil erosion from the redistribution of fallout 137Cs. *Soil Science Society of America Proceedings* **38**: 137–139. DOI: 10.2136/sssaj1974.03615995003800010042x

Roering JJ, Kirchner JW, Dietrich WE. 1999. Evidence for nonlinear, diffusive sediment transport on hillslopes and implications for landscape morphology. *Water Resources Research* **35**: 853–870. DOI: 10.1029/1998WR900090

Roering JJ, Kirchner JW, Sklar LS, Dietrich WE. 2001. Hillslope evolution by nonlinear creep and landsliding: An experimental study. *Geology* **29**: 143–146. DOI: 10.1130/0091-7613(2001)029<0143:HEBNCA>2.0.CO;2

Roering JJ, Perron JT, Kirchner JW. 2007. Functional relationships between denudation and hillslope form and relief. *Earth and Planetary Science Letters* **264**: 245–258. DOI: 10.1016/j.epsl.2007.09.035

Rogowski AS, Tamura T. 1965. Movement of ceasium-137 by runoff ,erosion and infiltration on the alluvial Captina silt loam. *Health Physics* **11**: 1333–1340.

Rouse JW, Haas RH, Schell JA, Deering DW. 1974. Monitoring vegetation systems in the Great Plains with ERTS. *Third Earth Resources Technology Satellite Symposium, NASA SP-351* **351**: 309–317.

Saco PM, Heras M las M. 2013. Ecogeomorphic coevolution of semiarid hillslopes: Emergence of banded and striped vegetation patterns through interaction of biotic and abiotic processes. *Water Resources Research* **49**: 115–126. DOI: 10.1029/2012WR012001

Shand CA, Cheshire M V, Smith S, Vidal M, Rauret G. 1994. Distribution of radiocaesium in organic soils. *Journal of Environmental Radioactivity* **23**: 285–302. DOI: 10.1016/0265-931X(94)90067-1

Soto J, Navas A. 2008. A simple model of Cs-137 profile to estimate soil redistribution in cultivated stony soils. *Radiation Measurements* **43**: 1285–1293. DOI: 10.1016/j.radmeas.2008.02.024

Stock JD, Dietrich WE. 2006. Erosion of steepland valleys by debris flows. *Geological Society of America Bulletin* **118**: 1125–1148. DOI: 10.1130/b25902.1

Sutherland RA. 1992. Caesium-137 estimates of erosion in agricultural areas. *Hydrological processes* **6**: 215–225. DOI: 10.1002/hyp.3360060209

Tamura T. 1964. Selective sorption reactions of caesium-137 with soil minerals. *Nuclear Safety* **5**: 262–268.

Tapponnier P, Xu ZQ, Roger F, Meyer B, Arnaud N, Wittlinger G, Yang JS. 2001. Oblique stepwise rise and growth of the Tibet Plateau. *Science* **294**: 1671–1677. DOI: 10.1126/science.105978

Walling D, Collins A, Sichingabula H. 2003. Using unsupported lead-210 measurements to investigate soil erosion and sediment delivery in a small

Zambian catchment. *Geomorphology* **52**: 193–213. DOI: 10.1016/S0169-555X(02)00244-1

Walling DE, He Q. 1992. Interpretation of caesium-137 profiles in lacustrine and other sediments: the role of catchment-derived inputs. *Hydrobiologia* **235-236**: 219–230. DOI: 10.1007/bf00026214

Walling DE, He Q. 1999. Improved models for estimating soil erosion rates from cesium-137 measurements. *Journal of Environmental Quality* **28**: 611–622. DOI: 10.2134/jeq1999.00472425002800020027x

Walling DE, He Q. 2000. The Global Distribution of Bomb-Derived 137cs Reference Inventories. International Atomic Energy Agency Report no. 10361/R0-R1

Walling DE, He Q, Quine TA. 1996. Use of fallout radionuclide measurements in sediment budget investigations. *Geomorphologie. Relief, Processus, Environnement* **3**: 17–27.

Walling DE, Quine TA. 1990. Calibration of caesium-137 measurements to provide quantitative erosion rate data. *Land Degradation & Rehabilitation* **2**: 161–175. DOI: 10.1002/ldr.3400020302

Walling DE, Zhang Y, He Q. 2011. Models for deriving estimates of erosion and deposition from fallout radionuclides (caesium-137, excess lead-210, and

beryllium-7) measurements and the development of user-friendly software for model implementation. In *Impact of Soil Conservation Measures on Erosion Control and Soil Quality.* IAEA-TECDOC-1665, International Atomic Energy Agency: Vienna; 11–33.

Wang CH, Huang B, Pan BT. 2010. Simulating and analyzing energy balance in Qilian Mountains. *Journal of Glaciology and Geocryology (in chinese)* **32**: 78–82.

Whipple KX, Tucker GE. 1999. Dynamics of the stream-power river incision model: Implications for height limits of mountain ranges, landscape response timescales, and research needs. *Journal of Geophysical Research B: Solid Earth* **104**: 17661–17674. DOI: 10.1029/1999JB900120

Wu FL, Fang XM, Ma YZ, Mark H, Volker M, An ZS, Miao YF. 2007. Plio–Quaternary stepwise drying of Asia: Evidence from a 3-Ma pollen record from the Chinese Loess Plateau. *Earth and Planetary Science Letters* **257**: 160–169. DOI: 10.1016/j.epsl.2007.02.029

Table 1 Study transects information and erosion rates

Site	Transect [3]	Elevation	Gradient	L_h [4]	*NDVI*	Mean Inventory [5]	Mean Erosion [6]
-	-	(m)	(m/m)	(m)	-	(Bq/m^2)	(mm/a)
AS (565) [1] (5684) [2]	AS24	3865	0.24	49	0.633	4136(1281 - 8403)	0.35(0.37 - 0.34)
	AS32	3701	0.32	48	0.649	3191(1493 - 5009)	0.57(0.59 - 0.54)
	AS36	3809	0.36	47	0.617	4357(1470 - 9681)	0.31(0.33 - 0.29)
	AS37	3640	0.37	47	0.741	4091(1297 - 6684)	0.37(0.39 - 0.35)
	AS53	3662	0.53	44	0.702	3894(1810 - 6516)	0.40(0.42 - 0.38)
MS (394) (4955)	MS16	2758	0.16	59	0.550	4161(2300 - 8940)	0.20(0.21 - 0.19)
	MS22	2929	0.22	93	0.612	4277(2334 - 7798)	0.17(0.18 - 0.16)
	MS36	2948	0.36	104	0.648	4017(695 - 8630)	0.25(0.26 - 0.23)
	MS44	2901	0.44	78	0.569	2816(1141 - 6606)	0.58(0.61 - 0.55)
	MS58	2987	0.58	61	0.546	3371(391 - 8454)	0.48(0.51 - 0.46)
MG (250) (4190)	MG25	2194	0.25	48	0.468	2901(1090 - 6234)	0.42(0.44 - 0.40)
	MG35	2194	0.35	47	0.471	2689(1476 - 4743)	0.46(0.48 - 0.43)
	MG43	2208	0.43	46	0.457	1819(820 - 4713)	0.80(0.84 - 0.76)
	MG54	2194	0.54	44	0.485	2740(517 - 5905)	0.52(0.55 - 0.49)
	MG68	2224	0.68	41	0.416	3372(274 - 6570)	0.35(0.36 - 0.33)
DG (235) (4098)	DG18	2114	0.18	49	0.458	3185(791 - 5479)	0.30(0.32 - 0.29)
	DG27	2124	0.27	48	0.455	3002(237 - 5077)	0.42(0.44 - 0.40)
	DG39	2131	0.39	47	0.464	3355(315 - 6914)	0.29(0.30 - 0.27)
	DG49	2121	0.49	45	0.452	3103(630 - 7382)	0.37(0.39 - 0.35)
	DG57	2140	0.57	43	0.451	2907(270 - 11175)	0.46(0.48 - 0.44)
	DG67	2165	0.67	42	0.460	1961(154 - 4244)	0.79(0.83 - 0.75)

[1] predicted mean annual rainfall (mm/a)

[2] corresponding reference inventory (Bq/m^2)

[3] transect names are sites with a subscript of their gradient

[4] transect length (L_h) is the planimetric coordinate of slope length measured parallel to the soil surface

[5] Note that the values in the brackets are the minimum inventory and the maximum inventory in each transect

[6] Note that the erosion rates in the brackets are calculated using the parameters for the upper/lower confidence bounds, left side values are calculated by the upper bound parameters, while right side values are calculated by the lower bound parameters

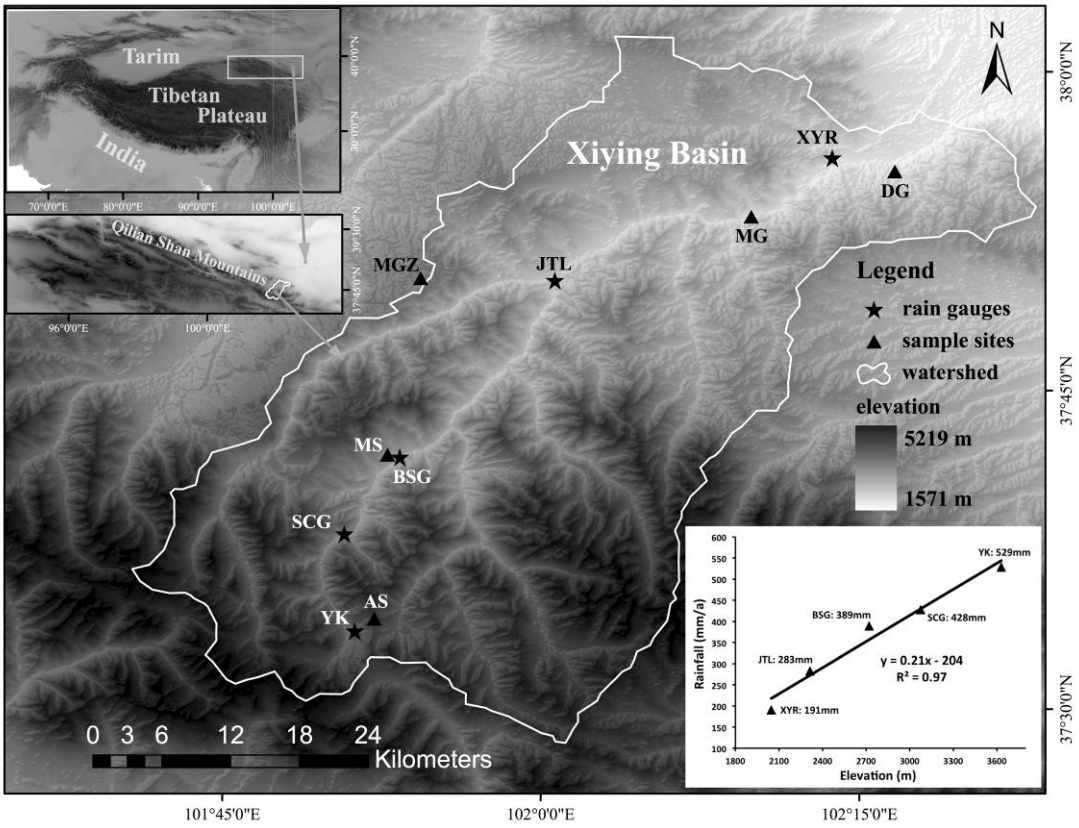

Figure 1. Shaded-relief map of Xiying Basin (Area ~1700 km^2) with locations of five weather stations (black solid stars, YK, SCG, BSG, JTL, XYR) and five ^{137}Cs sample sites (black solid triangles, MGZ, AS, MS, MG, DG). Note that MGZ is the reference site. Inset figure in southeast corner shows the plots of station elevations versus the recorded rainfall.

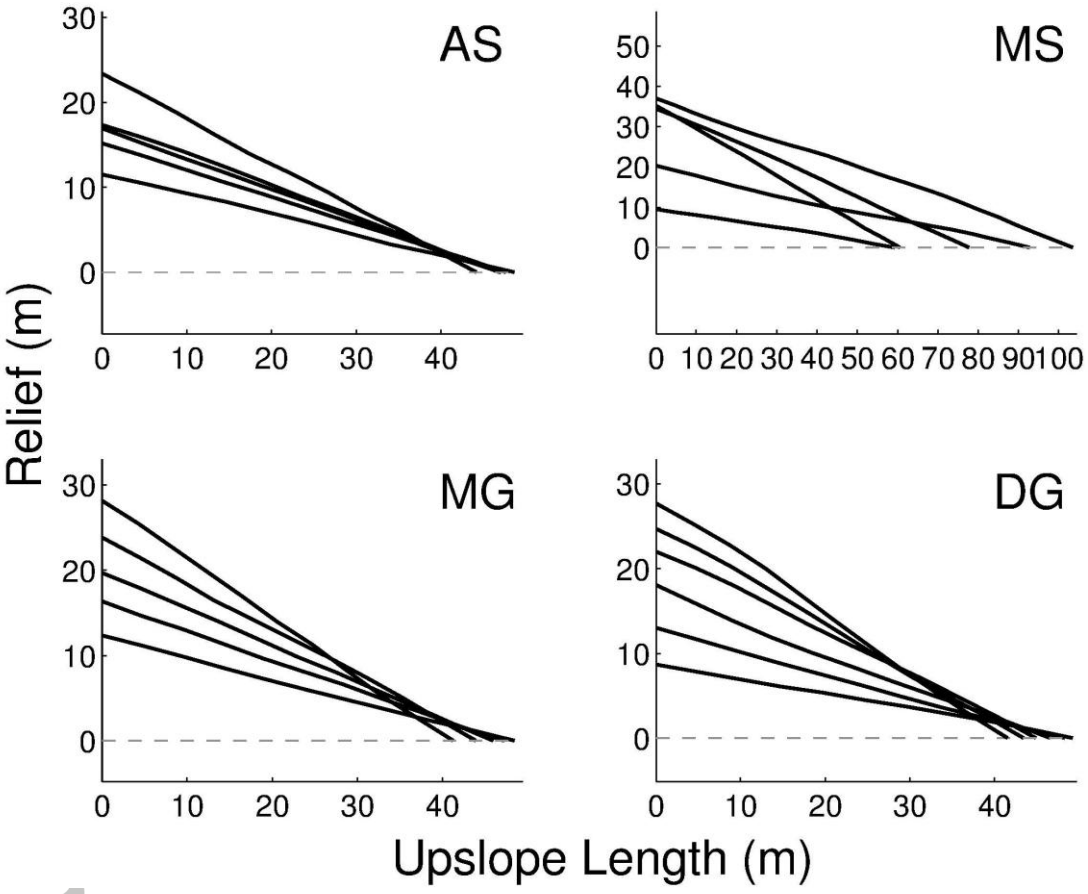

Figure 2. Topographic profiles of the 21 transects for the 4 study sites. Elevation (y-axis) is in metres above the base of the transect, upslope length (x-axis) is in metres from the ridge, transects always follow the path of steepest descent.

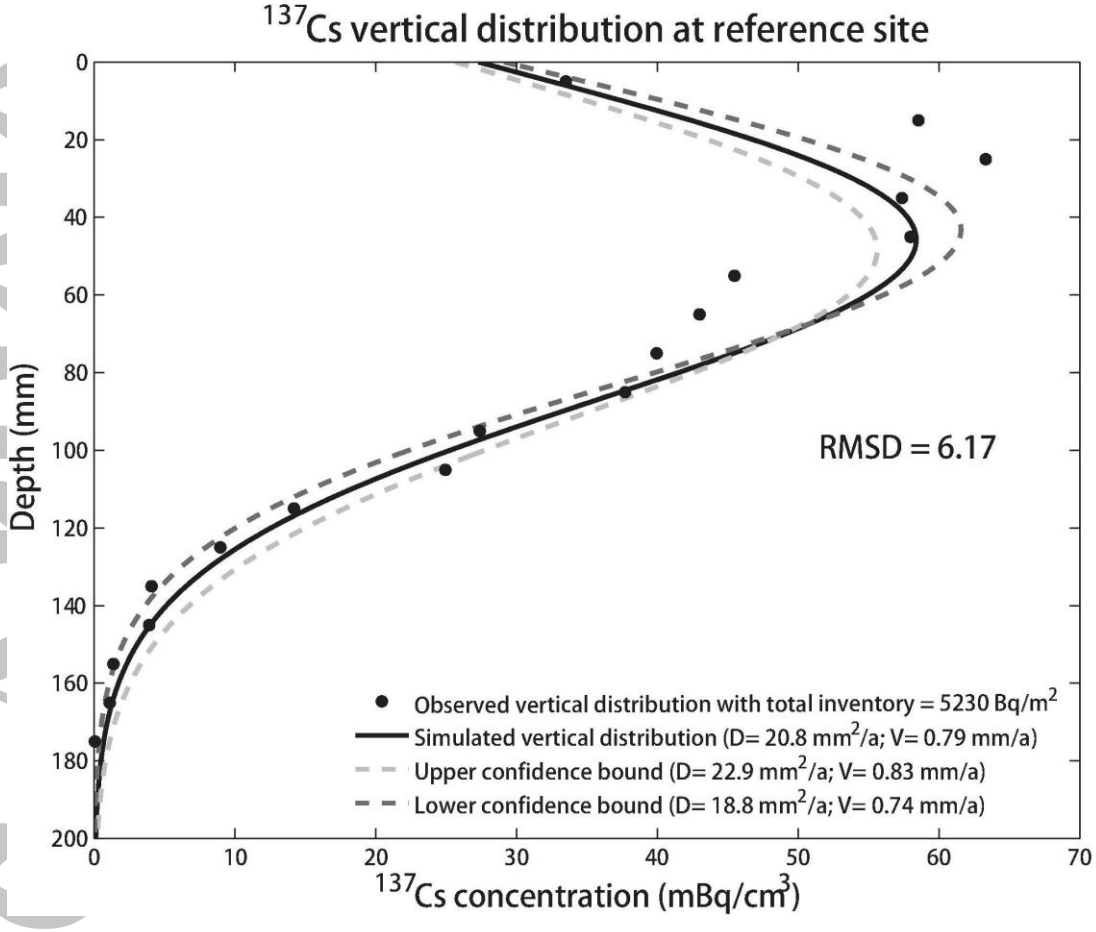

Figure 3. Observed vertical ^{137}Cs profile at reference site (points) with model simulated ^{137}Cs profile (solid line). Dashed lines show profile predictions using the upper (light gray) and lower (dark gray) 5% confidence bounds for the parameters *D* and *V*. The Root-Mean-Square Deviation (RMSD) represents the standard deviation of the differences between observed ^{137}Cs concentrations and the model predicted values.

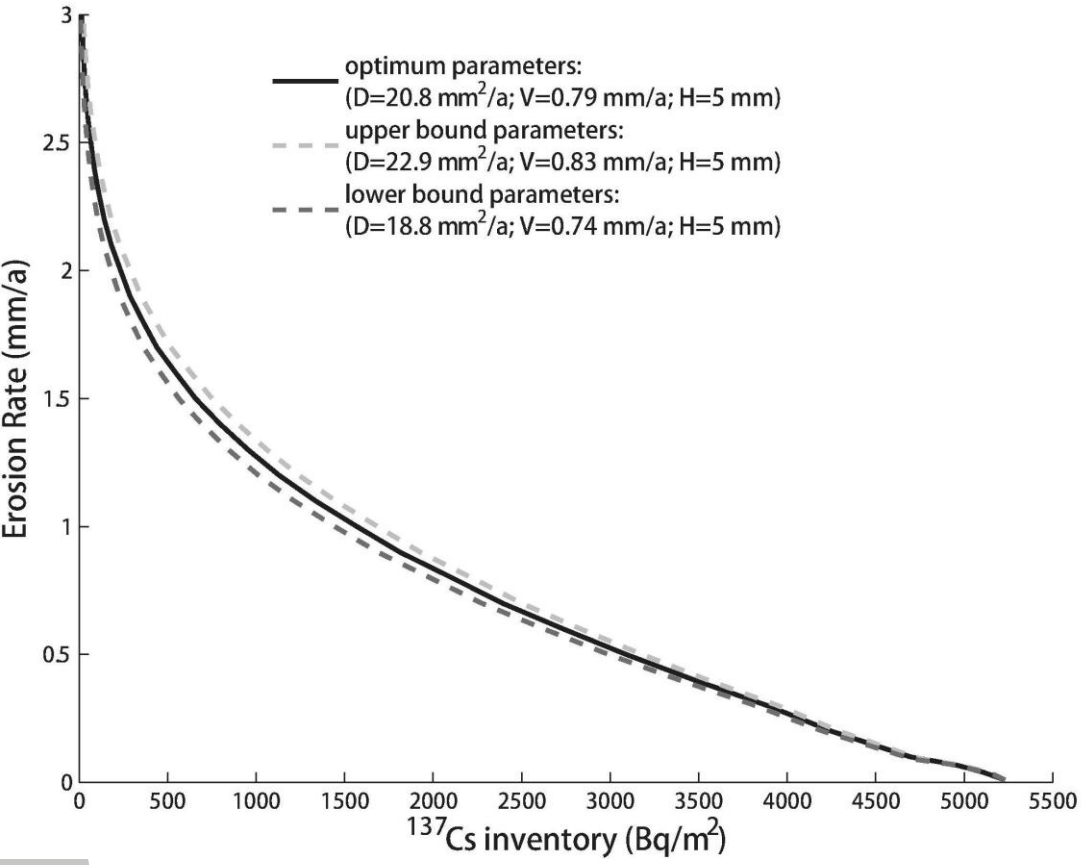

Figure 4. The relationship between soil erosion rates and the ^{137}Cs remaining in the inventory accounting for changing boundary conditions due to soil erosion (black solid line). The upper confidence bound (light gray dashed line) and lower confidence bound (dark gray dashed line) relationships are also shown in this figure. Note the plots were obtained with the reference inventory of 5230 Bq/m^2.

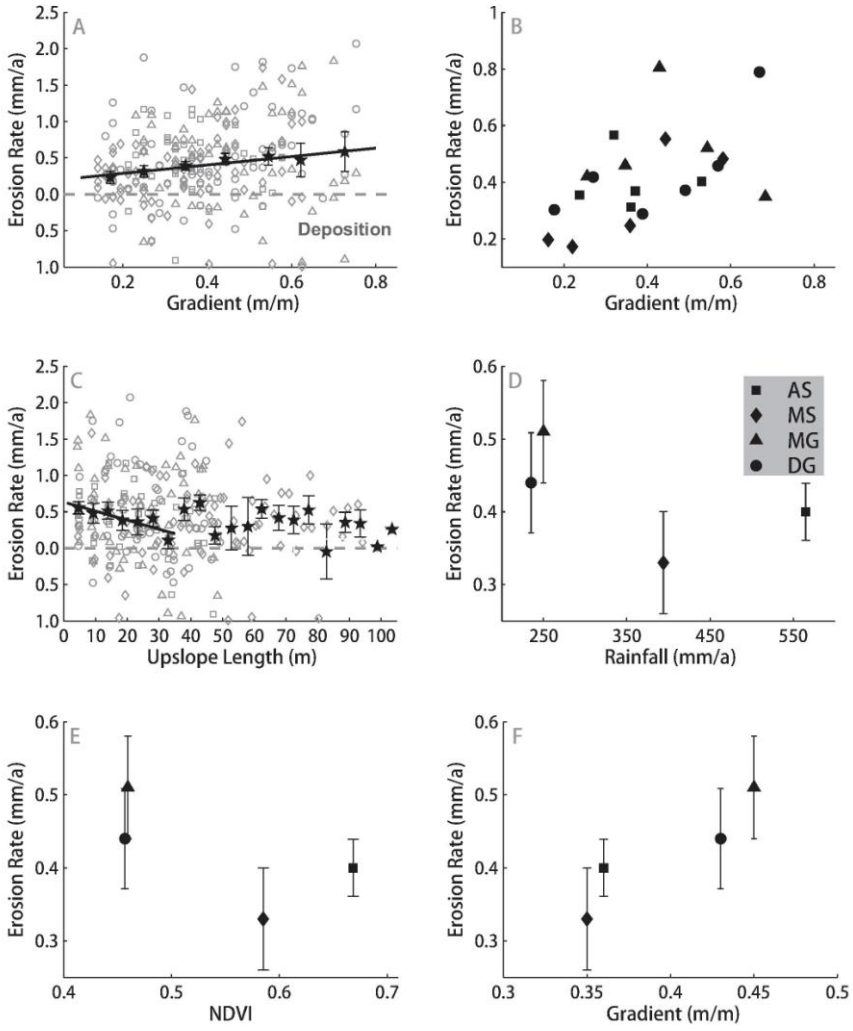

Figure 5. Scatter plots of ^{137}Cs erosion rates against potential controlling factors. A) shows the local gradient for all sample points (open symbols) with solid pentagrams showing average erosion rates for binned gradients (0.1 m/m bins). B) shows the relationship between transect-averaged erosion rates and gradients. C) shows the upslope length for all sample points (open symbols) with solid pentagrams showing average erosion rates for binned upslope lengths (5 m bins). D – F show the relationship between site-averaged erosion rates and rainfall (D), *NDVI* (E) and gradient (F), respectively. Markers styles label the data points from different study sites. Error bars in A, C, D, E and F are 1 standard error of the mean (SEM). In A and C, the erosion and deposition are both in positive values and separated by a light gray dashed line.

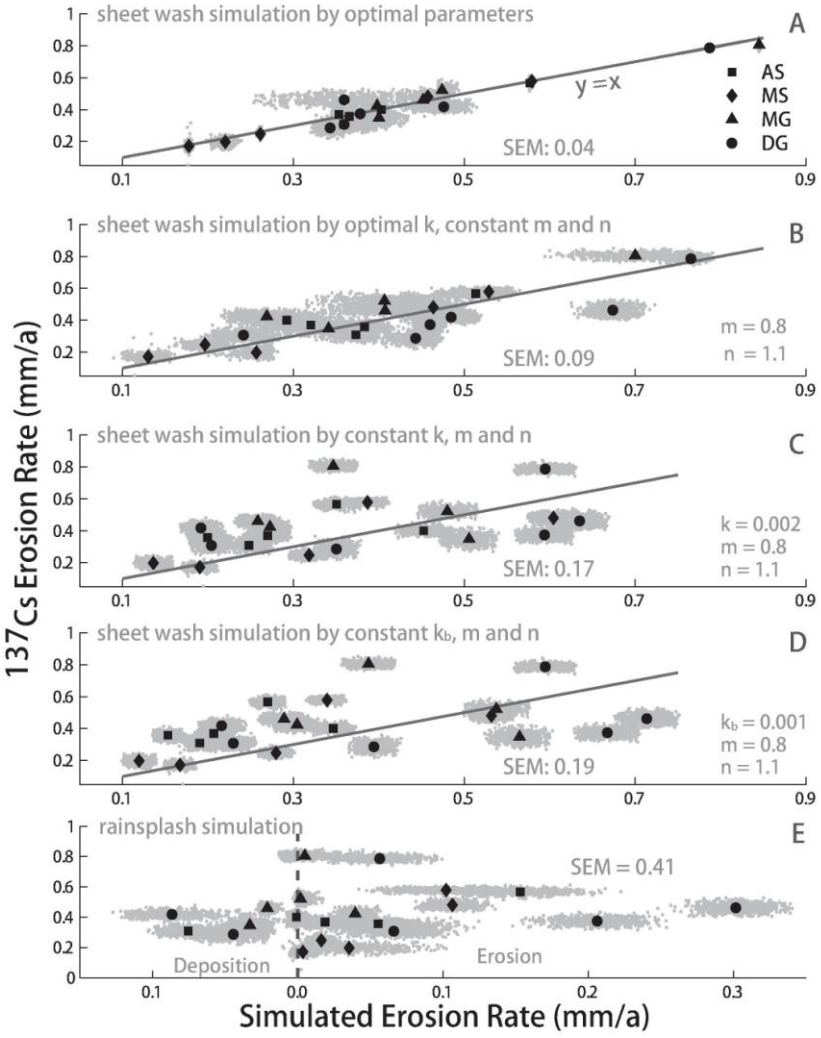

Figure 6. Simulated mean erosion against ^{137}Cs-derived mean erosion rates for the 21 transects. Plot A – D represent the results of overland flow simulation: (A) with optimal parameters (*k, m, n*) for each transect; (B) with constant exponents (m = 0.8 and n = 1.1) for all transects but optimal k for each transect; (C) with constant parameters (k = 0.002, m = 0.8, n = 1.1) for all transects using Eq. 4; (D) with constant parameters (k_b = 0.001, m = 0.8, n = 1.1) using Eq. 10. Plot E represents the simulated rainsplash erosion against ^{137}Cs-derived erosion. The light gray dots show individual results from 500 Monte Carlo simulation runs for each transect. Note that in plot E, erosion and deposition are both in positive values and separated by light gray dashed lines.

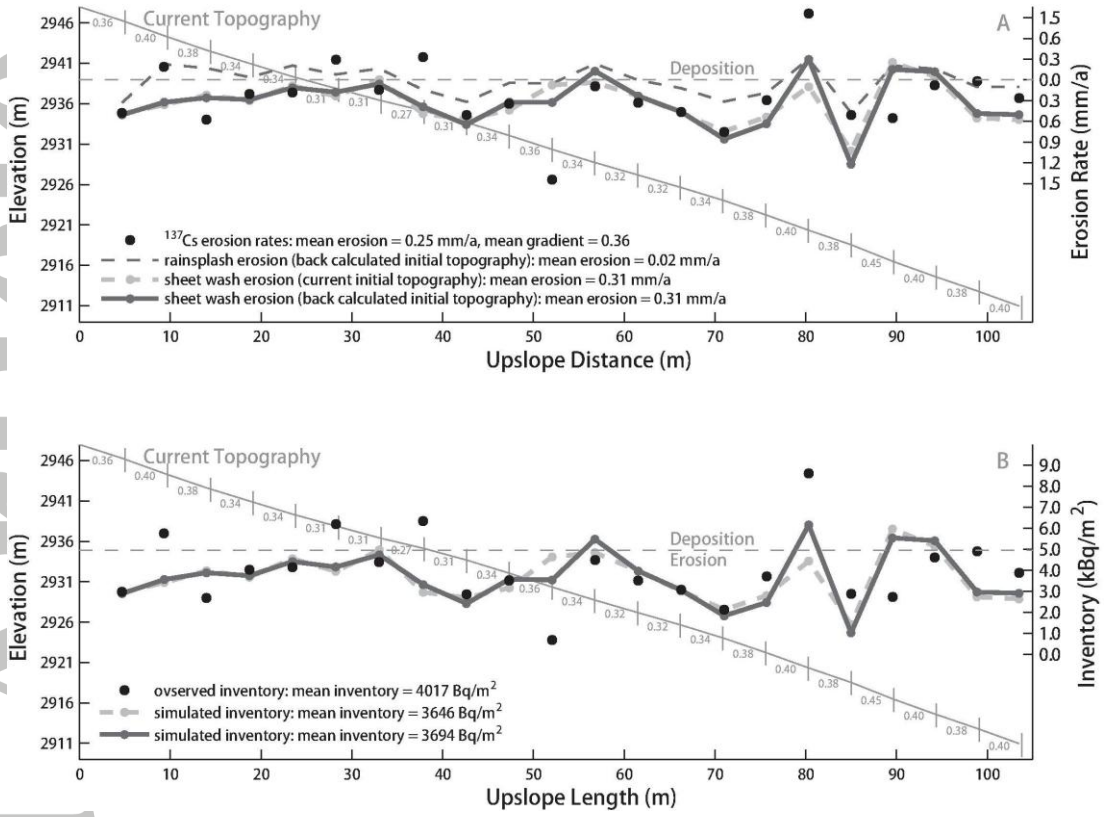

Figure 7. Topographic profile, erosion rates and ^{137}Cs inventory at transect MS36. (A) ^{137}Cs-derived erosion rates (solid points) and simulated erosion rates for rainsplash (dashed line) and sheet wash (lines with points). Note that erosion and deposition are both in positive values (right vertical axis), and separated by a light gray dashed line. (B) Observed ^{137}Cs inventories (solid points) and simulated inventories under sheet wash (lines with points). The parameter values used in this simulation are: k = 0.002, m = 0.8, n = 1.1, and d = 0.032 m^2/a. For the results from the other 20 transects see Figures S6-10 in supplementary information.

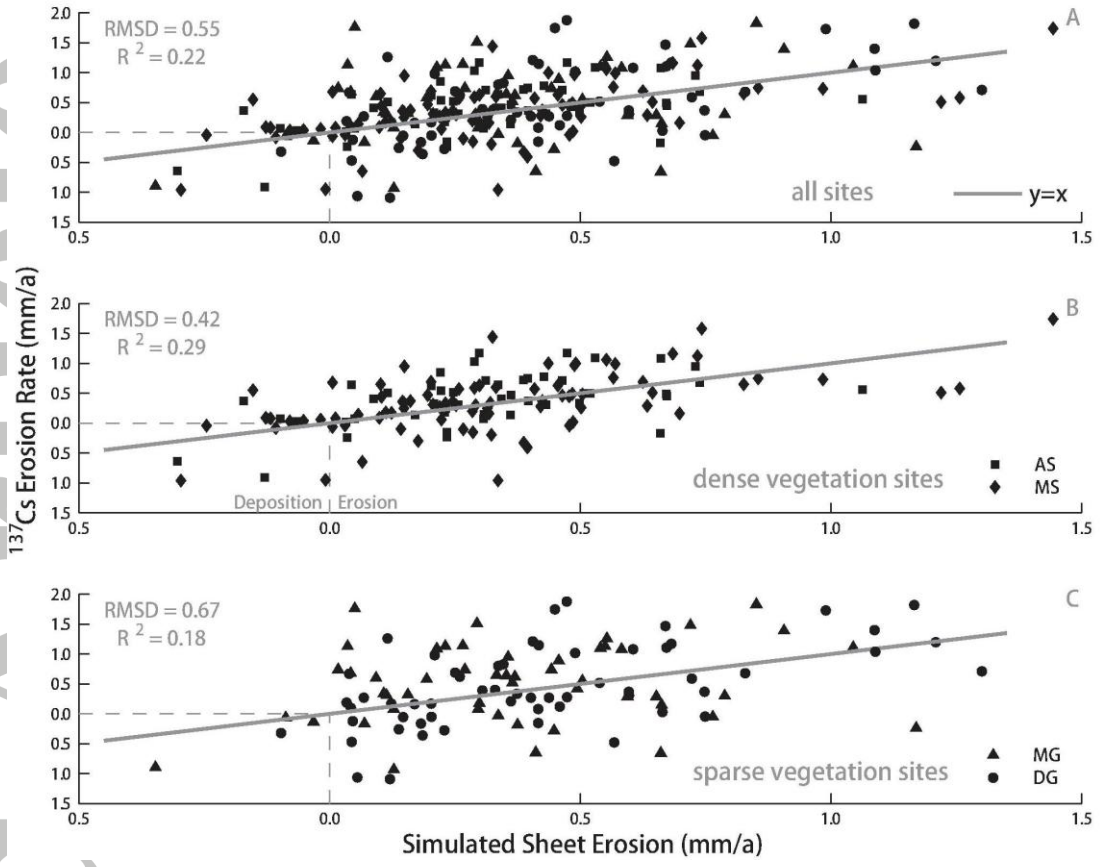

Figure 8. ^{137}Cs-derived erosion rates compared with simulated erosion rates at individual sample points. Simulated erosion is with constant parameters (k = 0.002, m = 0.8, n = 1.1) for all transects. Different marker styles indicate the data points from different study sites. (A) All sample points (21 transects); (B) sample points from the 10 transects under dense vegetation (AS and MS); (C) sample points from the 11 transects under sparse vegetation (MG and DG). Note that erosion and deposition are both in positive values and from zero up on y-axis and right on x-axis refers to deposition.